Journal of Cell Science 112, 1835-1842 (1999)
Printed in Great Britain © The Company of Biologists Limited 1999
JCS0395

Cellular expression of green fluorescent protein, coupled with high-resolution in vivo videomicroscopy, to monitor steps in tumor metastasis

George N. Naumov[1,4], Sylvia M. Wilson[4], Ian C. MacDonald[1], Eric E. Schmidt[1], Vincent L. Morris[1,2,3], Alan C. Groom[1], Robert M. Hoffman[5] and Ann F. Chambers[1,2,3,4,*]

Departments of [1]Medical Biophysics, [2]Microbiology and Immunology, and [3]Oncology, University of Western Ontario, London, Ontario, Canada N6A 5C1
[4]London Regional Cancer Centre, London, Ontario, Canada N6A 4L6
[5]AntiCancer, Inc., San Diego, CA 92111, USA
*Author for correspondence (e-mail: achambers@lrcc.on.ca)

Accepted 8 April; published on WWW 26 May 1999

SUMMARY

High resolution intravital videomicroscopy has provided a powerful tool for directly observing steps in the metastatic process, and for clarifying molecular mechanisms of metastasis and modes of action of anti-metastasis therapeutics. Cells previously have been identified in vivo using exogenously added fluorescent labels, limiting observations to a few cell divisions, or by natural markers (e.g. melanin) expressed only by specific cell types. Here we tested the utility of stable green fluorescent protein (GFP)-transfected cells for monitoring and quantifying sequential steps in the metastatic process. Using CHO-K1 cells that stably express GFP, we document the visualization and quantification by intravital videomicroscopy of sequential steps in metastasis within mouse liver, from initial arrest of cells in the microvasculature to the growth and angiogenesis of metastases. Individual, non-dividing cells, as well as micro- and macrometastases could clearly be detected and quantified, as could fine cellular details such as pseudopodial projections, even after extended periods of in vivo growth. We quantified the size distribution of micrometastases and their locations relative to the liver surface using 50 μm thick formalin-fixed tissue sections. The data suggest preferential growth and survival of micrometastases near the liver surface. Furthermore, we observed a small population of single cells that persisted over the 11 day observation period, which may represent dormant cells with potential for subsequent proliferation. This study demonstrates the advantages of GFP-expressing cells, coupled with real-time high resolution videomicroscopy, for long-term in vivo studies to visualize and quantify sequential steps of the metastatic process.

Key words: Green fluorescent protein (GFP), Metastasis, Pseudopodia, Angiogenesis, Mouse liver, Intravital videomicroscopy

INTRODUCTION

Despite recent advances in treatment of primary tumors, metastasis remains the major cause for failure in cancer treatment (Weinstat-Saslow and Steeg, 1994; Fidler and Ellis, 1994; Liotta and Stetler-Stevenson, 1993). By better understanding the mechanisms of the metastatic process, it will be possible to identify the steps that are most susceptible to therapeutic intervention (Woodhouse et al., 1997; Zetter, 1998; Chambers et al., 1999). To address questions regarding the in vivo formation of metastases, a way is needed to directly observe metastasis as it occurs over time. High resolution intravital videomicroscopy (IVVM) permits the study of events in the metastatic process that were previously inaccessible by commonly used in vivo and in vitro assays (Chambers et al., 1992, 1995; Morris et al., 1993; I. C. MacDonald et al., 1998). Although 'spontaneous' and 'experimental' end-point metastasis assays allow for quantification of the number and sizes of metastases in various organs, they do not provide information on how these metastases develop. IVVM provides an observation window which allows access to steps in hematogeous metastasis that previously were difficult to observe and impossible to quantify.

Visualization of tumor cells by IVVM requires that the cells carry a marker to distinguish them from the surrounding normal tissue. The naturally expressed marker melanin is extremely valuable for the detection of melanoma cells (Chambers et al., 1992; Luzzi et al., 1998); however, some cells may escape detection because of the heterogeneous expression of melanin within cell populations. Exogenous fluorescent markers have therefore been employed. Calcein-AM is a cytoplasmic marker that gives a clear outline of the cell profile (MacDonald et al., 1992) but is lost from the cells with time, limiting its use to a period of approximately 24 hours from the time of uptake into the cells. Fluorescent plastic nanospheres (Morris et al., 1994) are useful cell markers which do not fade with time but, since they are not distributed uniformly within cells, visualization of the cell boundary is difficult. Moreover, consecutive dilution of the label occurs with each cell division, rendering cells virtually undetectable after two to three

divisions. Clearly, what is needed is an endogenous tumor cell marker that is stably expressed over long periods of time in vivo by all cells of the population injected and by their progeny, permitting their detection by IVVM.

Transfection of tumor cells with green fluorescent protein (GFP) (Misteli and Spector, 1997) cDNA produces a heritable, stable cytoplasmic marker that allows cells to be detected for long term observations in vivo. To date, the use of GFP-expressing tumor cells has permitted visualization of individual metastatic cells and end-point spontaneous metastases in freshly excised organ specimens (Chishima et al., 1997a-c; T. J. MacDonald et al., 1998; Yang et al., 1998, 1999). It has also permitted quantification of the motility of tumor cells within primary tumors in the mammary fat pad, by means of in vivo time-lapse confocal microscopy (Farina et al., 1998). However, real-time monitoring by IVVM of sequential steps in the metastatic process over the long term, using GFP-expressing cells, has not (to our knowledge) been carried out previously.

In the present report we document the visualization and quantification by IVVM of sequential steps in the metastatic process of GFP-expressing CHO-K1 cells within mouse liver, from initial arrest of cells in the microvasculature to their eventual growth into macroscopic tumors in which angiogenesis is occurring. We were able to clearly observe details such as cytoplasmic projections, even many days after injection of the cells, and to follow the growth of micrometastases over extended periods of time; furthermore, individual non-dividing cells were readily detectable long after injection. The use of GFP-expressing tumor cells constitutes a powerful new tool to further expand the capabilities of high resolution intravital videomicroscopy, in order to study cellular and molecular details of the metastatic process.

MATERIALS AND METHODS

Cell culture

CHO-K1-GFP is a Chinese hamster ovary cell line previously transfected (Chishima et al., 1997b) with the pED-mtx^r expression vector containing the highly-fluorescent S56T variant (GFP-S56T) of the wild-type GFP gene and the DHFR gene as a selectable methotrexate (MTX)-resistance marker. CHO-K1-GFP cells were maintained (37°C, 5% CO_2 humidified atmosphere) in Dulbecco's modified Eagle's medium (DMEM; Canadian Life Technologies Inc., Burlington, ON) supplemented with 10% fetal calf serum (FCS; Canadian Life Technologies Inc.). The cells were routinely subcultured at a ratio of 1:10 in selective medium containing 1.5 μM MTX (Sigma, St Louis, MO) and were maintained in culture for no more than 5 passages. Cells from subconfluent monolayers were harvested by trypsinization and resuspended in DMEM/10% FCS to a final concentration of 2×10^6 cells/ml. Prior to injection, it was determined by epi-fluorescence microscopy that ≥95% of the cells excluded ethidium bromide, indicating that membrane integrity was maintained (Weiss et al., 1992; Morris et al., 1993).

Stability of GFP expression

To characterize the stability of GFP fluorescence over time, cells were grown with or without MTX-selective medium and were passaged every fourth day over a 24-day period. After each cell passage fluorescence intensity was assessed by flow cytometry (Epics XL-MCL, Coulter, Miami, FL). For each sample 10,000 cell counts were performed in duplicate.

Intravital videomicroscopy

Female SCID mice, 6-7 weeks of age (Charles River, St Constant, Quebec), were cared for in accordance with standards of the Canadian Council on Animal Care, under an approved protocol of the University of Western Ontario Council on Animal Care. Mice were anesthetized using a ketamine/xylazine mixture (1.6 mg of ketamine and 0.08 mg of xylazine per 15 g body mass) administered by intraperitoneal injection. A suspension of 3×10^5 CHO-K1-GFP cells in 0.15 ml of DMEM supplemented with 10% FCS was injected via a mesenteric vein to target the liver, as previously described (Morris et al., 1993). Temgesic analgesic (0.1 mg/kg body weight) was administered subcutaneously as mice awoke and 18 hours after surgery.

Mice were examined by IVVM (Chambers et al., 1995; I. C. MacDonald et al., 1998) immediately (up to 90 minutes) after injection of cells or 1, 2, 3, 4, 7, 9, and 11 days later. The animals were anesthetized with sodium pentobarbitol (60 mg/kg i.p.), after which a portion of a liver lobe was exposed and the mouse placed on a viewing platform on the stage of an epi-fluorescence inverted microscope (Nikon Diaphot TMD). Oblique transillumination was provided by a fiber optic light source to enhance cell contrast and epi-illumination (450-490 nm) was used to excite GFP. Real-time images obtained using a video camera with extended red sensitivity (Panasonic, WV 1550), were viewed on a video monitor and recorded on SVHS videotape. The animal's temperature was monitored and maintained at 37°C using a heat lamp. Anesthesia was maintained with supplemental administration of sodium pentobarbitol as required.

Histology

Mice were sacrificed by anesthetic overdose after IVVM. The livers were fixed in 10% neutral buffered formalin (pH 7.6) and sectioned (~50 μm thick) using a Vibratome Series 1000 sectioning system (Technical Products International, St Louis, MO) as described previously (Luzzi et al., 1998). Tissue was not paraffin-embedded because GFP fluorescence is lost during treatment with organic solvents (Chalfie et al., 1994). Sections were examined microscopically using the green fluorescence of tumor cells to identify them and to quantify tumor number, tumor size, and shortest distance between the tumor center and the periphery of the liver. To eliminate double- and triple-counting of the same micrometastasis in serial tissue sections, unbiased stereological correction was used (Weibel, 1979).

Statistical analysis

Statistical analyses were performed using a Statistical Analysis Software, Version 6 for Windows (SAS Institute Inc., Cary, NC). To assess the relationship between two specific factors, regression functions were obtained by linear regression analyses. Data on distribution of tumor foci with respect to the liver surface were analyzed using three parameters for comparison: mean distance, standard deviation, and maximum values. A level of $P<0.05$ was regarded as statistically significant.

RESULTS

Stability of GFP fluorescence intensity in vitro

The fluorescence intensity of CHO-K1-GFP cells maintained in the presence vs absence of MTX over a 24 day period in vitro was quantified (Fig. 1). For cells grown in the presence of MTX the median fluorescence intensity at day 3 was 105 (arbitrary units) compared to 81 units at day 24. In the absence of MTX, cells showed a median fluorescence intensity of 95 units, similar to that of cells maintained under selective pressure at day 24. Thus the in vitro fluorescence intensity of the cells was sufficiently stable to permit detection in vivo, even in the

absence of selective pressure. Non-fluorescent cells were not detected among cells maintained with or without MTX.

Cell arrest in liver sinusoids, extravasation, and early growth of micrometastases

Cytoplasmic expression of GFP permitted IVVM identification of individual tumor cells (10-15 μm in diameter) and their morphology against the faint yellow autofluorescence of the liver tissue and the dark red appearance of the blood vessels. GFP permits resolution of a high level of detail of cellular morphology at all stages of the metastatic process. At 90 minutes after injection, all observed cancer cells remained within sinusoidal vessels near terminal portal venules in acinar zone 1 (Fig. 2A). Occasionally cells near branch points were forced into several sinusoids at once, resulting in odd shape deformations (Fig. 2A). Twenty-four hours after initial arrest, most cells had completed extravasation and others were in the process of extravasating. Pseudopodial projections extending through the vascular wall from tumor cells were observed during this process, and some extravasated cells were found wrapped around the abluminal surfaces of vessels. Other extravasated cells were seen to extend long slender projections to the avascular region immediately below the liver capsule. These projections could be as long as 60 μm and GFP permitted resolution of their detailed morphology, such as the bifurcation seen in Fig. 3A. Extravasated tumor cells, located within the liver tissue between sinusoids (Fig. 2B), remained viable upon completion of the extravasation process, as indicated by the persistence of their green fluorescence.

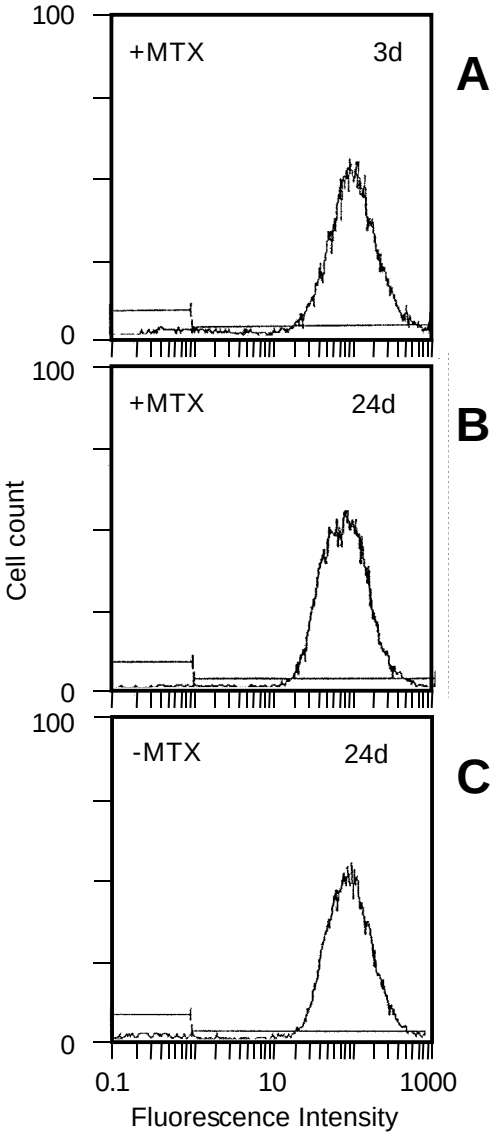

Fig. 1. Stability of GFP fluorescence intensity in vitro. Fluorescence intensity was analyzed by flow cytometry of CHO-K1-GFP cells suspended in medium. (A) Fluorescence intensity distribution of cells maintained in media containing MTX (1.5 μM) as a selection pressure against non-GFP-expressing cells. The analysis was performed 3 days after initial cell plating. (B) Fluorescence intensity profile of the same cell population 24 days after the initial reading. The cells were continuously maintained in MTX (1.5 μM). No significant changes were observed in the general shape and position of the distribution. (C) Fluorescence intensity profile of CHO-K1-GFP cells originating from the initially observed (A) cell population, but continuously grown after that point in the absence of MTX. This mimics the selection-free in vivo environment of the mouse liver. Readings were taken every 4 days and did not differ from the beginning and end-point data presented.

Multicellular micrometastases present by day 4 (Fig. 2C), ranged in diameter from 20 to 380 μm and at higher magnification individual cells within them could be clearly seen by IVVM, especially at the tumor periphery. Views of one of these micrometastases taken at two different focal depths (‘optical slicing’) are shown in Fig. 3B,C. At a deeper plane of focus (Fig. 3B), the center of the metastasis is clear but the peripheral cells appear out of focus. In contrast, at a plane nearer the surface of the liver (Fig. 3C) the same peripheral cells appear in sharper focus than the interior cells, indicating that these peripheral cells had invaded the avascular layer located just below the liver capsule. Details of individual pseudopodia from micrometastases were clearly visible (Fig. 3B,C). Larger micrometastases separated by normal tissue are present by day 9, many of them showing pseudopodial projections extending from their periphery into the surrounding tissue (e.g. Fig. 2D). Solitary individual tumor cells were also present in the tissue at this and later times, visible under IVVM solely because of their GFP fluorescence. Three such cells detected in close proximity (≥50 μm) to two metastases at day 11 are shown in Fig. 3D. Based on the observed blood flow directions within vessels of this area, it is unlikely that these cells had spread via the vasculature from the adjacent tumors. Such cells could represent undivided cells remaining from the original injection or might have migrated within the liver parenchyma from the adjacent metastases.

Development of tumor microvasculature

Microvessels were first seen within the metastases at day 11. By fluorescence illumination the vessels appeared dark against the green fluorescence of the tumor tissue and had a highly distorted configuration, as illustrated in Fig. 3E. By transillumination at higher magnifications, the movement of individual blood cells was clearly seen using IVVM. Red blood cell (RBC) motion was measured in vessels that passed from normal to tumor tissue. Typically, relatively steady flow (e.g. 53.6 μm/second ±2.2 (s.d.) in a 10.5 μm vessel) became far more sluggish within the tumor tissue, with complete stasis in some branches. Fig. 4A,B illustrates the highly irregular

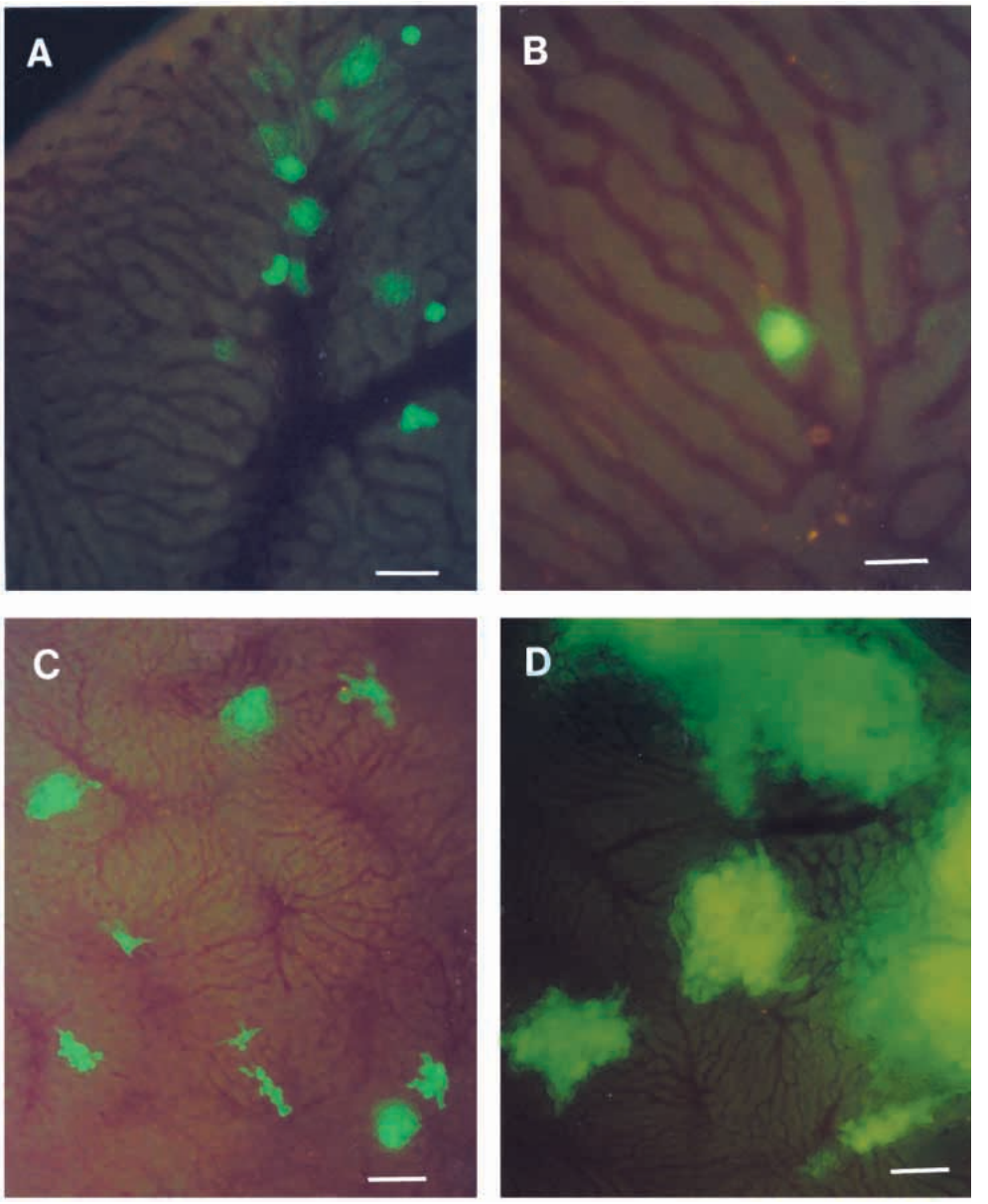

Fig. 2. Sequential steps of metastasis in mouse liver, visualized in vivo by IVVM of GFP-expressing CHO-K1 cells. (A) Intravascular cells arrested due to size restriction within mouse liver sinusoids near terminal portal venules (acinar zone 1), visualized one hour after injection. Tumor cells appear bright green against the background of dark red blood vessels and pale yellow autofluorescence of the liver tissue. Bar, 50 μm. (B) Extravasated cell observed 24 hours after injection, located out in liver tissue between sinusoids. By IVVM it could be seen that blood flow had resumed within these sinusoids. Bar, 25 μm. (C) Overview showing small micrometastases 4 days after cell injection. Note the variety of shapes and sizes, as well as pseudopodial projections at the periphery of most micrometastases. Bar, 100 μm. (D) Larger micrometastases separated by normal tissue are present at day 9, many of them exhibiting pseudopodial projections extending from their periphery into the surrounding tissue. Bar, 100 μm. Views A to D are all photomicrographs taken with a 35 mm camera, using epifluorescence plus a low level of transillumination.

morphology often seen, and Table 1 gives the corresponding diameters and RBC velocities at selected locations.

Size distribution and locations of micrometastases

Quantification of the size distribution of micrometastases (Fig. 5) and their locations relative to the liver surface (Fig. 6) was performed following the real-time IVVM observations, using 50 μm thick formalin-fixed tissue sections. Such quantification was made possible through the identification of single cells and micrometastases in these sections via their expression of GFP. Only single cells were present up to day 1 but by day 2, small micrometastases of 2-4 cells accounted for 11.8% of the total tumor foci observed (Fig. 5). By day 3, the proportion of single cells had decreased to 38% of the tumor foci observed, and by day 11 this proportion had decreased to only 2%. The numbers of micrometastases increased dramatically by day 3: approximately 40% of the total foci consisted of small micrometastases 20-80 μm in diameter, and a further 20% had reached diameters up to 140 μm. However, by day 4 these numbers had changed to 15% and 65%, respectively, indicating that significant growth of the micrometastases had occurred in the meantime. By day 7, micrometastases up to 380 μm diameter were found, although the great majority were ≤260 μm in size. By day 9 the range of diameters was even greater, with a few micrometastases up to 560 μm being found. By day 11 the median size of micrometastases had obviously increased further (Fig. 5), but the range of diameters was smaller, with micrometastases measuring 140-380 μm.

The initial distribution of tumor cells immediately after injection (Fig. 6, top panel) showed cells located throughout the organ, and these data are consistent with a random distribution. The volume of tissue available for trapping cells decreases with distance from the surface (see Fig. 6 inset) and, therefore, for a random distribution of cells the heights of the bars should decrease with distance from the surface, as was found. This pattern was typical for tumor foci (single cells and

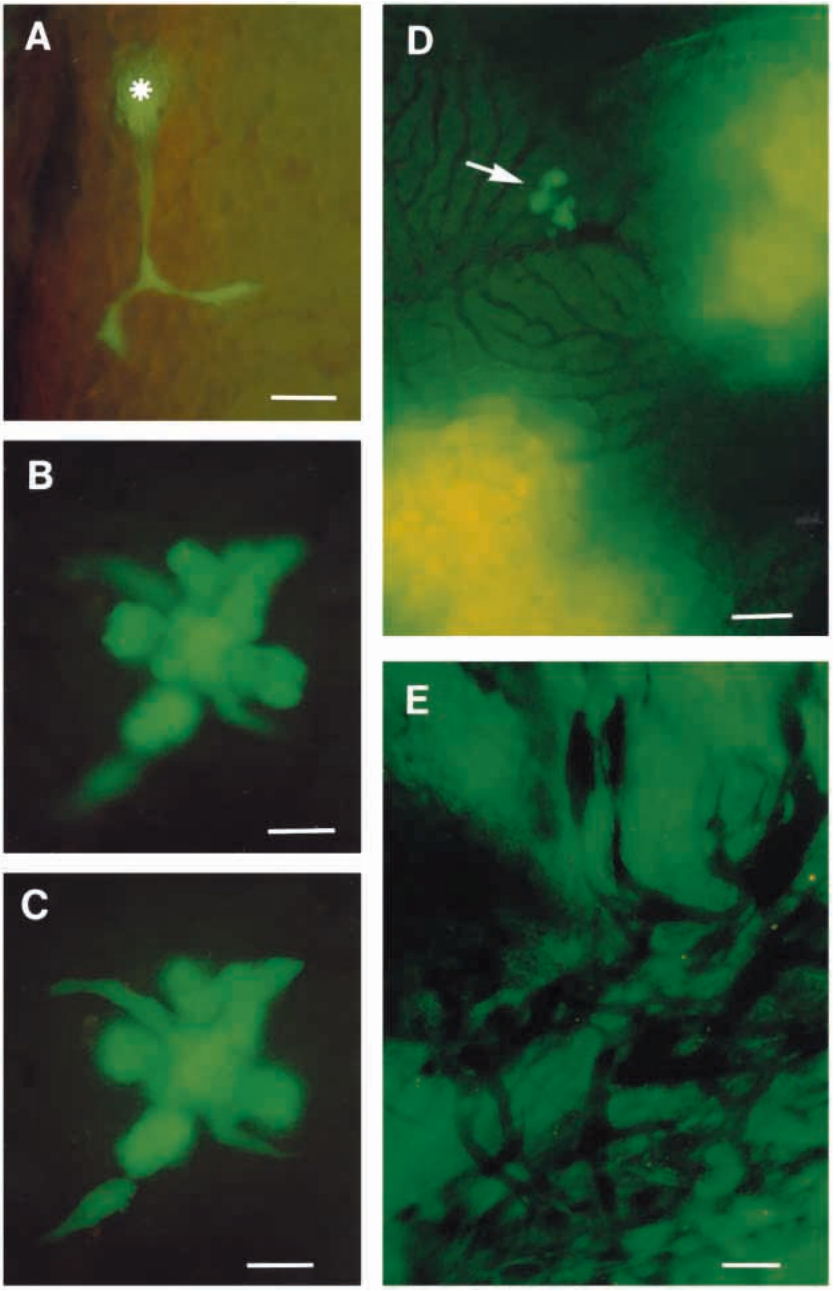

Fig. 3. Morphological observations by IVVM: interactions of cells and metastases with liver microenvironment. (A) An extravasated CHO-K1-GFP cell at day 1, in the process of migration to the hepatocyte layer in subcapsular region. Cell body (*), slightly below the plane of focus, extends a long, bifurcated pseudopodial projection up towards the liver surface. (Viewed by epifluorescence plus transillumination.) Bar, 25 μm. (B,C) Micrometastasis at day 4 observed by epifluorescence alone, at two different focal depths ('optical slicing'). (B) Viewed at a deeper plane of focus, center of micrometastasis is sharply defined but peripheral cells appear out of focus. Bar, 25 μm. (C) Viewed nearer to the liver surface, peripheral cells are more sharply defined than cells at the center, indicating that the peripheral cells had invaded the hepatocyte layer located just below the liver capsule. Bar, 25 μm. (D) Solitary tumor cells (→) present in normal liver tissue at day 11, in close proximity to two metastases. (Viewed by epifluorescence plus transillumination.) Bar, 50 μm. (E) Highly distorted microvasculature within metastasis at day 11, viewed by epifluorescence alone. Blood vessels appear dark against GFP-fluorescent background of tumor tissue. Bar, 25 μm. Views A to E are photomicrographs taken with a 35 mm camera.

micrometastases) up to day 4, but by day 7 a different distribution had emerged: tumor foci were found only within ~400 μm of the surface, whereas at greater depths (down to ~900 μm, the center of the organ) they had disappeared. This change in distribution was statistically significant, based on linear regression analysis using three parameters from the data shown in Fig. 6 for comparison: mean distance (P=0.037), standard deviation (P=0.013), and maximum values (P=0.018). Thus, the data suggest a preferential growth and survival of micrometastases near the liver surface and failure of cells located more centrally to survive.

Table 1. Diameters and flow velocities at specified locations, for tumor vessel in Fig. 4

Location	Diameter (μm)	RBC velocity (μm/s)±s.d.
1	60.9	17.4±0.7
2	53.7	31.3±7.1
3*	N/A	0
4	34.1	44.0±4.6

*Location 3 represents a shallow stagnant 'pocket' extending alongside the flow stream at location 2.

DISCUSSION

In the past, GFP has been used to detect metastatic cells in freshly excised tissue samples (Chishima et al., 1997a-c; T. J. MacDonald et al., 1998; Yang et al., 1998, 1999), and for studies of cell motility within primary tumors in the mammary fat pad by in vivo time-lapse confocal microscopy (Farina et al., 1998). The success of these studies suggested that the use

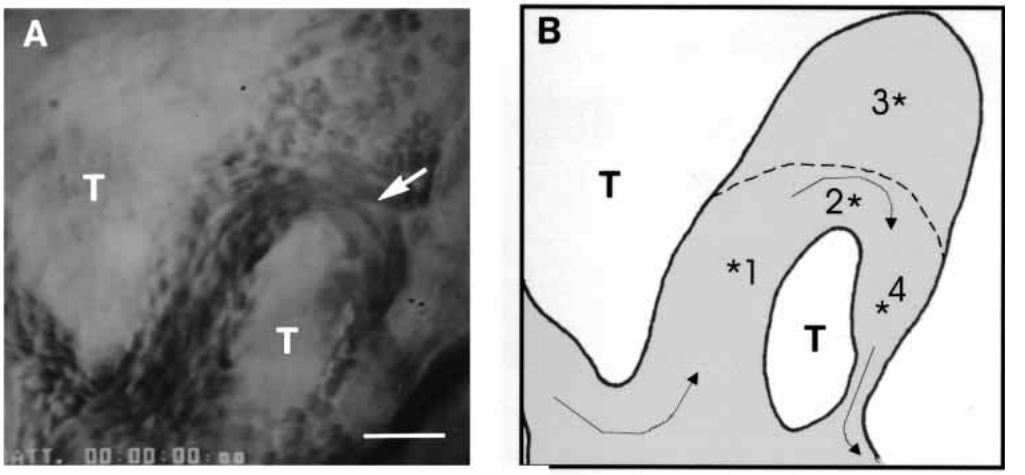

Fig. 4. Tumor microvasculature observed by IVVM. (A) View of a typical intra-tumoral vascular loop, recorded using a black/white video camera (epifluorescence plus transillumination). Greatly increased contrast between RBCs and tumor tissue is achieved due to background illumination from the GFP fluorescence. Note characteristic variations in vessel diameter and RBC content. Individual RBCs may be clearly distinguished in areas of low flow, but appear blurred (→) where flow is more rapid. Bar, 50 μm. (B) Schematic of image A indicating areas 1-4 where measurements of diameter and RBC velocity were made (see Table 1). Blood flow direction is represented by arrows. Note that area 3 (above the dotted line) is a vascular pocket containing stationary RBCs. Tumor tissue, T.

of GFP-expressing cells would facilitate in vivo investigations of the metastatic process by IVVM, which until now have been limited in certain respects by the cell labeling techniques available. Utilization of GFP as a cell label for in vivo experiments requires that cells be stably transfected, expressing GFP over the long term. The CHO-K1-GFP cells used in the present study exhibited stable fluorescence (as demonstrated by flow cytometry) even after 24 days maintenance in vitro in medium deprived of selective pressure**;** moreover, the entire cell population remained fluorescent under these conditions. This indicates suitability of the cells for long-term use in vivo, and we demonstrate here the advantages of GFP-expressing cells for visualization and quantification, by real-time IVVM, of sequential steps in the metastatic process.

GFP-expressing tumor cells injected into the portal circulation could be seen clearly at subsequent stages of metastasis: initial arrest of cells in the liver microvasculature, extravasation, growth into micrometastases, and continued growth into macroscopic tumors in which angiogenesis took place. Previously, such in vivo visualization of tumor cells had been possible only by using exogenous markers such as Calcein-AM or fluorescent nanospheres, and/or the natural marker melanin in melanoma cells (I. C. MacDonald et al., 1992, 1998; Luzzi et al., 1998). Calcein-AM showed the detailed morphology of individual cells but disappeared within ~24 hours. Fluorescent nanosphere labeling lasted longer, until diluted out by 2-3 cell divisions; however, visualization of cell boundaries was difficult because of non-uniform distribution of nanospheres throughout the cytoplasm. Limitations of the endogenous marker melanin include its expression by only specific cell types (e.g. melanoma); furthermore, some cells may escape detection because of the heterogeneous expression

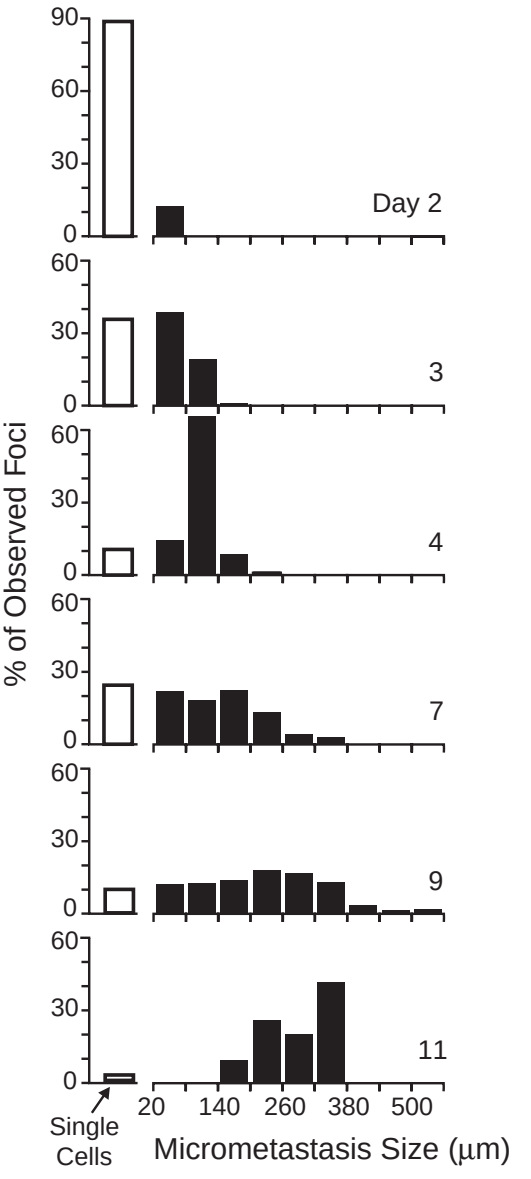

Fig. 5. Survival and growth of single cells and micrometastases. GFP made possible the visualization and quantification of single cells and small micrometastases which would have been difficult or impossible to detect by other methods. The percentage of the total observed foci which consisted of single undivided cells (white bars) decreased with time, from 100% at day 1 (not shown) to only 2% at day 11. Micrometastases (black bars) increased in size progressively over the 11 day period, as shown by the changes in size distribution.

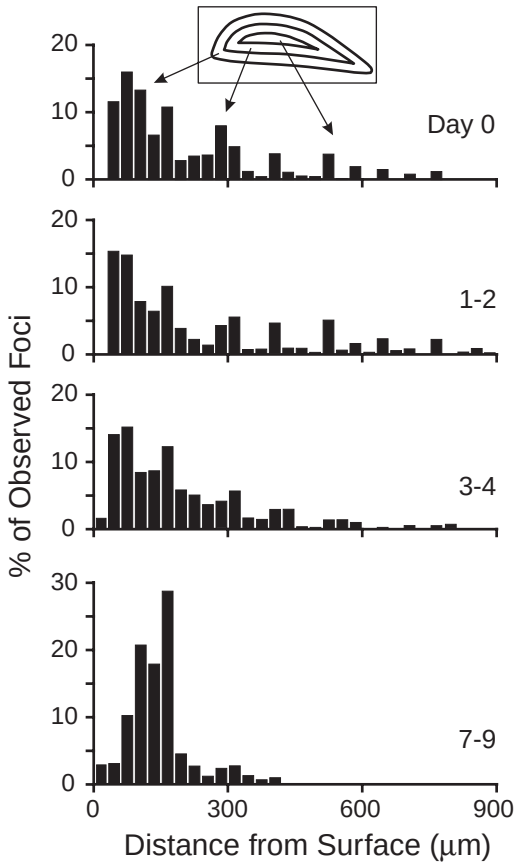

Fig. 6. Distribution of tumor foci observed (single cells and micrometastases), in terms of depth below the liver surface. The data for day 0 are consistent with a random distribution of cells throughout the organ. The volume of tissue available for initial cell arrest in the microcirculation decreases with distance from the surface (shown in the schematic cross section of a liver lobe, see inset) and, therefore, for a random distribution of cells the heights of the bars should decrease linearly with distance, reaching zero at the center of the organ. This pattern was typical for tumor foci up to day 4, but by day 7 a different distribution had emerged: tumor foci were found only within 400 μm of the surface, whereas at greater depths they had disappeared. This change in distribution was statistically significant, based on linear regression analysis using the following parameters: mean distance (P=0.037), standard deviation (P=0.013), and maximum values (P=0.018).

of melanin within cell populations. In contrast, use of GFP as a cytoplasmic marker (which can be transfected into any cell type of interest) enabled us to visualize in vivo both the general outlines of cells and fine morphological details such as long slender pseudopodial projections, for extended periods of time.

Pseudopodial projections from solitary individual cells were more clearly visible with GFP than any we have seen previously using other markers, and never before have we seen bifurcations of pseudopodia in vivo (Fig. 3A). Furthermore, to our knowledge pseudopodial projections from cells around the periphery of micrometastases have not previously been detected in vivo (except for melanoma in chick embryo chorioallantoic membrane: Chambers et al., 1992), and the present study using GFP revealed such projections in micrometastases of all sizes. In larger micrometastases these projections were often directed particularly toward other micrometastases close by, implying some form of interaction between them. The fact that GFP-expressing single cells and micrometastases could be seen so clearly by IVVM and also in formalin fixed thick tissue sections opened the way, for the first time, for detailed quantification of the growth of micrometastases and their locations relative to the liver surface, and how these parameters changed with time. Of particular interest was the finding that micrometastases seem to show preferential growth and survival near the liver surface (confirming the results of Dingemans et al., 1985, 1994) and that those that are located more centrally fail to survive. This raises the question of whether the tissue close to the liver surface contains preferentially the factors necessary for metastatic growth. A further advantage of GFP-expressing cells is the increased contrast between brightly fluorescent tumor tissue and blood vessels within it. The ability to visualize and quantify blood vessel development in metastases in vivo will greatly facilitate studies of angiogenesis and the testing of effects of anti-angiogenic agents on metastatic development.

We recently showed that, contrary to what is generally believed, a significant population of melanoma cells remain within the liver tissue by 13 days after injection, as solitary, dormant cells, and that most small micrometastases that formed by day 3 failed to continue to grow (Luzzi et al., 1998). Detection of these solitary cells and micrometastases was only possible due to their melanin content (and nanosphere labeling for undivided cells), and we could not have done the study on other cancer cell types. However, transfection and expression of GFP makes possible such studies on any cancer cell type of interest. Here we have used CHO-K1 cells, and the present findings together with our recent data (Luzzi et al., 1998) point to the existence of a previously unappreciated phenomenon. We have identified a population of single undivided cells surviving in the tissue up to two weeks after injection. These apparently dormant cells could have the potential to be activated at a later time and commence growth. If this situation also occurs clinically, these dormant cells will represent a critically important population to understand and control. The present study shows that GFP is superior to previously used cancer cell markers and, used in combination with intravital videomicroscopy of intact organs, GFP allows for reliable in vivo detection and quantification of sequential steps in metastasis. This method should provide a powerful tool to further our understanding of mechanisms involved in metastasis and angiogenesis, and allow for real-time monitoring and evaluation of the effects of therapeutic agents targeted at specific key steps of metastasis.

We thank Larry W. Stitt (Biostatistics Support Unit, Department of Epidemiology and Biostatistics, University of Western Ontario) for assistance with the statistical analysis, and Michael Kenney (London Health Sciences Centre) for assistance with the flow cytometry. This research was supported by grant #8133 from the National Cancer Institute of Canada, and by an award from the Lloyd Carr-Harris Foundation.

REFERENCES

Chalfie, M., Tu, Y., Euskirchen, G., Ward, W. W. and Prasher, D. C. (1994). Green fluorescent protein as a marker for gene expression. *Science* **263**, 802-805.

Chambers, A. F., Schmidt, E. E., MacDonald, I. C., Morris, V. L. and

Groom, A. C. (1992). Early steps in hematogenous metastasis of B16F1 melanoma cells in chick embryos studied by high-resolution intravital videomicroscopy. *J. Nat. Cancer Inst.* **84**, 797-803.

Chambers, A. F., MacDonald, I. C., Schmidt, E. E., Koop, S., Morris, V. L., Khokha, R. and Groom, A. C. (1995). Steps in tumor metastasis: new concepts from intravital videomicroscopy. *Cancer Metast. Rev.* **14**, 279-301.

Chambers, A. F., MacDonald, I. C., Schmidt, E. E., Morris, V. L. and Groom, A. C. (1999). Preclinical assessment of anti-cancer therapeutic strategies using in vivo videomicroscopy. *Cancer Metast. Rev.* **17**, 263-269.

Chishima, T., Miyagi, Y., Wang, X., Baranov, E., Tan, Y., Shimada, H., Moossa, A. R. and Hoffman, R. M. (1997a). Metastatic pattern of lung cancer visualized live and in process by green fluorescence protein expression. *Clin. Exp. Metast.* **15**, 547-552.

Chishima, T., Miyagi, Y., Wang, X., Yamaoka, H., Shimada, H., Moossa, A. R. and Hoffman, R. M. (1997b). Cancer invasion and metastasis visualized in live tissue by green fluorescent protein expression. *Cancer Res.* **57**, 2042-2047.

Chishima, T., Yang, M., Miyagi, Y., Li, L., Tan, Y., Baranov, E., Shimada, H., Moossa, A. R., Penman, S. and Hoffman, R. M. (1997c). Governing step of metastasis visualized in vitro. *Proc. Nat. Acad. Sci. USA* **94**, 11573-11576.

Dingemans, K. P., Van Spronsen, R. and Thunnissen, E. (1985). B16 melanoma metastases in mouse liver and lung: I. Localization. *Invasion Metast.* **5**, 50-60.

Dingemans, K. P., van den Bergh Weerman, M. A., Keep, R. F. and Das, P. K. (1994). Developmental stages in experimental liver metastases: relation to invasiveness. *Int. J. Cancer* **57**, 433-439.

Farina, K. L., Wyckoff, J. B., Rivera, J., Lee, H., Segall, J. E., Condeelis, J. S. and Jones, J. G. (1998). Cell motility of tumor cells visualized in living intact primary tumors using green fluorescent protein. *Cancer Res.* **58**, 2528-2532

Fidler, I. J. and Ellis, L. M. (1994). The implications of angiogenesis for the biology and therapy of cancer metastasis. *Cell* **79**, 185-188.

Liotta, L. A. and Stetler-Stevenson, W. G. (1993). Principles of molecular cell biology of cancer: cancer metastasis. In *Cancer: Principles and Practice of Oncology* (ed. V. T. DeVita Jr, S. Hellman and S. A. Rosenberg), pp. 134-149. Lippincott, Philadelphia.

Luzzi, K. J., MacDonald, I. C., Schmidt, E. E., Kerkvliet, N., Morris, V. L., Chambers, A. F. and Groom, A. C. (1998). Multistep nature of metastatic inefficiency: Dormancy of solitary cells after successful extravasation and limited survival of early micrometastases. *Am. J. Pathol.* **153**, 865-873.

MacDonald, I. C., Schmidt, E. E., Morris, Chambers, A. F. and Groom, A. C. (1992). Intravital videomicroscopy of the chorioallantoic microcirculation: a model system for studying metastasis. *Microvasc. Res.* **44**, 185-199.

MacDonald, I. C., Schmidt, E. E., Morris, V. L., Groom, A. C. and Chambers, A. F. (1998). In vivo videomicroscopy of experimental hematogenous metastasis: cancer cell arrest, extravasation and migration. In *Motion Analysis of Living Cells* (ed. D. R. Soll and D. Wessels), pp. 263-288. Wiley-Liss, Inc, Toronto.

MacDonald, T. J., Tabrizi, P., Shimada, H., Zlokovic, B. V. and Laug, W. E. (1998). Detection of brain tumor invasion and micrometastasis in vivo by expression of enhanced green fluorescent protein. *Neurosurgery* **43**, 1437-1443.

Misteli, T. and Spector, D. L. (1997). Applications of the green fluorescent protein in cell biology and biotechnology. *Nature Biotech.* **15**, 961-964.

Morris, V. L., MacDonald, I. C., Koop, S., Schmidt, E. E., Chambers, A. F. and Groom, A. C. (1993). Early interactions of cancer cells with the microvasculature in mouse liver and muscle during hematogenous metastasis: videomicroscopic analysis. *Clin. Exp. Metast.* **11**, 377-390.

Morris, V. L., Koop, S., MacDonald, I. C., Schmidt, E. E., Grattan, M., Percy, D., Chambers, A. F. and Groom, A. C. (1994). Mammary carcinoma cell lines of high and low metastatic potential differ not in extravasation but in subsequent migration and growth. *Clin. Exp. Metast.* **12**, 357-367.

Weibel, E. R. (1979). Profile size and particle size. In *Stereological Methods: Practical Methods for Biological Morphometry*, vol. 1 (ed. E. R. Weibel), pp. 51-60. Academic Press, Inc, New York.

Weinstat-Saslow, D. and Steeg, P. S. (1994). Angiogenesis and colonization in the tumor metastatic process: basic and applied advances. *FASEB J.* **8**, 401-407.

Weiss, L., Nannmark, U., Johansson, B. R. and Bagge, U. (1992). Lethal deformation of cancer cells in the microcirculation: a potential rate regulator of hematogenous metastasis. *Int. J. Cancer.* **50**, 103-107.

Woodhouse, E. C., Chuaqui, R. F. and Liotta, L. A. (1997). General mechanisms of metastasis. *Cancer* **80**, 1529-1537**.**

Yang, M., Hasegawa, S., Jiang, P., Wang, X., Tan, Y., Chishima, T., Shimada, H., Moossa, A. R. and Hoffman, R. M. (1998). Widespread skeletal metastatic potential of human lung cancer revealed by green fluorescent protein expression. *Cancer Res.* **58**, 4217-4221**.**

Yang, M., Jiang, P., Sun, F. X., Hasegawa, S., Baranov, E., Chishima, T., Shimada, H., Moossa, A. R. and Hoffman, R. M. (1999). A fluorescent orthotopic bone metastasis model of human prostate cancer. *Cancer Res.* **59**, 781-786.

Zetter, B. R. (1998). Angiogenesis and tumor metastasis. *Annu. Rev. Med.* **49**, 407-424**.**